INTERNATIONAL JOURNAL FOR NUMERICAL AND ANALYTICAL METHODS IN GEOMECHANICS, VOL. 20, 191–208 (1996)

RESPONSE OF A LAYERED ELASTIC MEDIUM TO A MOVING STRIP LOAD

MANJRIKER GUNARATNE*

Department of Civil and Enivornmental Engr., Univ. of South Florida, Tampa, FL, USA

AND

ODELL SANDERS, III†

Umpqua National Park, U.S. Forest Service, Roseburg, OR, USA

SUMMARY

Analytical determination of stresses and deformations caused by moving loads is vital to foundation and pavement designs. In current applications, moving loads are often approximated to be vertical impact loads. In this work, however, a live load is modelled as a uniform distribution of normal or shear stresses in actual motion. Then, a layer stiffness approach utilizing linear elasticity is followed in determining the surface and interior deformations due to the live load. By superimposing the two solutions for normal and shear surface stresses, the new approach can be made to provide an approximate solution to the problem of evaluating stresses and deformations caused by a wide wheel load rolling on a layered elastic system. Although elastic solutions in general are inadequate to explain the more significant consequences of pore pressure generation and dissipation in the soil subgrade, these results can certainly be useful to examine the shearing effects of wide rolling wheels on the asphalt layer and immediate settlement of the subgrade. It is found that the dynamic effects of a smoothly rolling wide load are significant at relatively low wheel velocities compared to those of shear waves in the subgrade and base.

KEY WORDS: foundation design; pavement design; layer-stiffness technique; moving strip load

INTRODUCTION

Simple methods to predict the stresses and deflections due to loads moving on layered elastic media are scarce. The objective of this paper is to introduce a layer-stiffness-based technique to determine the response of an elastic layered medium to a moving strip load. Kausel and Roesset[1] and Kausel and Peek[2] presented a simple technique based on layer stiffnesses to determine the displacements and stresses due to dynamic loads on or within layered elastic media. Kausel[3] applied the above methodology to predict the response of a layered elastic medium to a *stationary* strip footing subjected to a vertical or horizontal harmonic load. However, so far this method has not been extended to determine the response of a layered system to a load in actual motion. Hence, in the work presented here, the authors predict the response of a layered elastic medium to a horizontally or vertically loaded strip load translating at a constant velocity. The load in motion is modelled as a moving uniform distribution of normal or shear stresses.

Since flexible pavements are often modelled as layered elastic system, the layer stiffness method has found several applications in flexible pavement evaluation research in recent years. Use in

*Associate Professor
†Operations Engineer

CCC 0363–9061/96/030191–18

Received 9 June 1994
Revised 18 August 1995

Road Rater excitation analysis,[4] and Falling Weight Deflectometer analysis[5] are some of them. In another related work involving a moving vehicle[6], the wheel load was modelled as a stress pulse.

A unique feature of the technique presented in this paper is that it can be utilized as an approximation to examine the pavement response to vertical or horizontal strip loads in actual motion. Moreover, by invoking the principle of superposition and using a coefficient of rolling friction, the two load cases (normal and shear) can be made to simulate the rolling effect of a wide load. The formulations and results given in the ensuing sections illustrate how the response at any depth of the layered system can be conveniently predicted in terms of *single space–time variable* using fast fourier transformation. It is also shown that the numerical results are in agreement with the closed-form solutions available for static loading conditions.

SUMMARY OF THE LAYER STIFFNESS PROCEDURE

The segment of the layer stiffness procedure pertinent to the present formulation is summarized in the following steps:

Step 1. Discretize the flexible pavement system in the direction of layering in formulate a stiffness matrix for each layer j $[K^j]$, in terms of elastic and dampling properties:

$$[\bar{P}] = [K^j][\bar{U}] \tag{1}$$

where $[P]$ is the stress vector (in the frequency domain) defined below in terms of the shear (τ) and normal stresses (σ) on the two horizontal layer interfaces (boundaries) as indicated by subscripts 1 and 2 (Figure 1):

$$[\bar{P}] = [\tau_{xz1}, \tau_{yz1}, i\sigma_{z1}, -\tau_{xz2}, -\tau_{yz2}, -i\sigma_{z2}]^T \tag{2}$$

Further, $[U]$ is the corresponding deflection vector (in the frequency domain) defined by displacements shown in Figure 1 as

$$[\bar{U}] = [u_{x1}, u_{y1}, iu_{z1}, u_{x2}, u_{y2}, iu_{z2}]^T \tag{3}$$

For plane strain conditions, $[K^j]$ is defined in Kausel and Roessat (1981) in terms of L, ρ, G and h, the Lame's constant, mass density, shear modulus and the layer thickness, respectively. The transcendental expressions for stiffness matrices can be simplified to algebraic expressions by using sufficiently small layer thicknesses according to the procedure developed by Lysmer and Waas[7]. The principal advantages of this simplification is the ability to obtain closed-form solutions for the resulting deflections. However, since the authors employ a numerical solution procedure, such simplified and approximate stiffness matrices are not essential. Furthermore, use of the original stiffness matrices will preclude the need for very fine layer discretization.

Step 2. Assemble the individual stiffness matrices to form the global stiffness matrix

$$[K] = \sum_j [K^j] \tag{4}$$

Step 3. Since the above stiffness matrices are derived in the frequency–wave number domain, transform the imposed (known) dynamic stresses to the same domain. This is accomplished by a Fourier transformation:

$$\overline{P(\omega, k)} = \int_{-\infty}^{\infty} \int_{-\infty}^{\infty} P(t, x)\, e^{-i(\omega t - kx)}\, dx\, dt \tag{5}$$

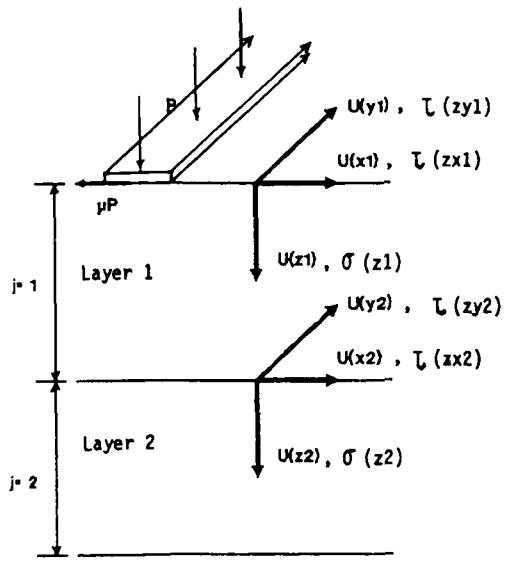

Figure 1. Stress/deflection notation for layer stiffness method

Step 4. Solve for the deflections in the frequency–wave number domain using regular matrix inversion:

$$[\overline{U(w,k)}] = [K]^{-1}[\overline{P(w,k)}] \tag{6}$$

Step 5. Transform the above deflections back to the time–space domain using inverse Fourier transformation:

$$U(t,x) = \frac{1}{4\pi^2}\int_{-\infty}^{\infty}\int_{-\infty}^{\infty}\overline{U(w,k)}\,e^{i(wt-kx)}\,dw\,dk \tag{7}$$

SIMULATION OF A MOVING LINE LOAD

The above procedure is now applied to investigate the dynamic effects of a translating strip load on a layered elastic system such as a flexible pavement, which comprises of an asphaltic surface layer (designated as the pavement), a strengthening base layer and the subgrade. In the theoretical development, the live load on the pavement surface is modelled as a moving pressure step function imposing normal as well as shear stresses due to friction (Figure 2). If the load translates past a certain location designated as origin of the X-axis at time $t = 0$, then, the stresses acting on the pavement surface can be described by the following expressions:

$$\tau_{xz} = -\mu p[ux - Vt + a) - u(x - Vt - a)] \tag{8a}$$

$$\tau_{yz} = 0 \tag{8b}$$

$$\tau_z = p[u(x - Vt + a) - u(x - Vt - a)] \tag{8c}$$

where u is the unit step function, V the rolling speed, μ the coefficient of rolling friction and p the tire pressure.

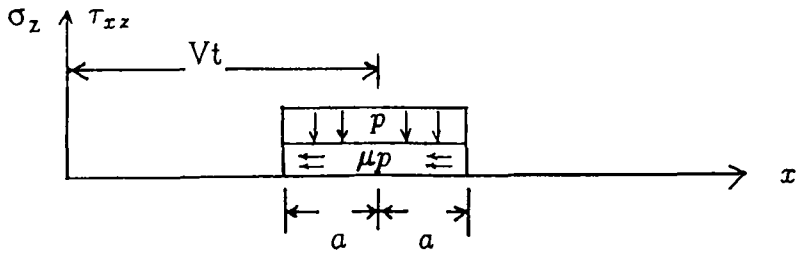

Figure 2. Normal and shear stress distribution on the surface

MODELLING OF THE FLEXIBLE PAVEMENT

In the ensuing formulation, the subscript j $(1, \ldots, i, i+1, \ldots, n, n+1)$ is used to designate the *global* location of the top surface of the layer j. Accordingly, top surface of the pavement, top surface of the subgrade, and bottom boundary of the subgrade are defined by $j = 1$, $i + 1$ and $n + 1$, respectively.

The bottom boundary of the subgrade must be selected at a depth where the surface effects are minimal, thereby undergoing negligible deflection. On the other hand, if the pavement system is constructed on a (infinitely) hard material like bedrock, the subgrade/bedrock interface will automatically satisfy this condition.

Furthermore, the superscripts, p, b and s are used to identify the pavement, based and the subgrade material, respectively. As an example, (1)–(3) can be applied to the top pavement layer to obtain the following local stiffness equation in global co-ordinates:

$$\begin{bmatrix} \overline{P_1} \\ \overline{P_2} \end{bmatrix} = \begin{bmatrix} K_{11}^{p} & K_{12}^{p} \\ K_{21}^{p} & K_{22}^{p} \end{bmatrix} \begin{bmatrix} \overline{U_1} \\ \overline{U_2} \end{bmatrix} \tag{9}$$

where $[P_1]$, $[U_1]$ and $[P_2]$, $[U_2]$ are the respective contributions from the two layer interfaces towards the stress and deflection vectors as defined in (2) and (3). The four separate $[K]$'s in (9) are the corresponding 3×3 partitions of the main $6 \times$ stiffness matrix in (1) for the topmost pavement layer. The latter is defined in Reference 1.

Similarly, the following local stiffness equation applies to the top layer of the subgrade bounded by the interfaces $i + 1$ and $i + 2$,

$$\begin{bmatrix} \overline{P_{i+1}} \\ \overline{P_{i+2}} \end{bmatrix} = \begin{bmatrix} K_{i+1,i+1}^{s} & K_{i+1,i+2}^{s} \\ K_{i+2,i+1}^{s} & K_{i+2,i+2}^{s} \end{bmatrix} \begin{bmatrix} \overline{U_{i+1}} \\ \overline{U_{i+2}} \end{bmatrix} \tag{10}$$

Moreover, for the bottom layer of the subgrade bounded by the surfaces n and $n + 1$, the stiffness equation can be written as

$$\begin{bmatrix} \overline{P_n} \\ \overline{P_{n+1}} \end{bmatrix} = \begin{bmatrix} K_{n,n}^{s} & K_{n,n+1}^{s} \\ K_{n+1,n}^{s} & K_{n+1,n+1}^{s} \end{bmatrix} \begin{bmatrix} \overline{U_n} \\ \overline{U_{n+1}} \end{bmatrix} \tag{11}$$

As state above, since the surface $n + 1$ is unaffected by the rolling wheel,

$$\overline{U_{n+1}} = 0 \tag{11a}$$

which leaves n free boundaries, thus reducing the global degrees of freedom to $3n$. The global stiffness matrix for the entire pavement system can be assembled by algebraically summing the local stiffness partitions having the same global subscripts. This is identical to the assembly procedure adopted in structural analysis. Therefore, the banded global stffiness matrix in (12) corresponds to that in (4) in Step 2 of the layer stiffness procedure:

$$\begin{bmatrix} \overline{P_1} \\ \vdots \\ \overline{P_n} \end{bmatrix} = [K_G] \begin{bmatrix} \overline{U_1} \\ \vdots \\ \overline{U_n} \end{bmatrix} \tag{12}$$

As noted above, (8) expresses the stress vector acting on the surface 1 of the pavement system in the x–t domain. This enables $[P_1]$ to be obtained by the Fourier transform (FT) of the stress vector in (8) as

$$[\overline{P_1}] = \mathrm{FT} \begin{bmatrix} -\mu p[u(x - Vt + a) - u(x - Vt - a)] \\ 0 \\ ip[u(x - Vt + a) - u(x - Vt - a)] \end{bmatrix} \tag{13}$$

The use of (5) to operate the Fourier transform in (13) will be illustrated in the section describing the numerical procedure. As for the interior surfaces ($j = 2, \ldots, n - 1$),

$$[\overline{P_j}] = \begin{bmatrix} 0 \\ 0 \\ 0 \end{bmatrix} \tag{14}$$

since there are no external forces in the pavement interior under usual circumstances.

Now, with the force vector known, Steps 4 and 5 of the layer stiffness procedure can be executed to determine the deflection vector $[U]$.

NUMERICAL METHODOLOGY

Fourier transform of the stress vector

The Fourier transform in (13) can be determined in the following manner by substituting for $P(x,t)$ from (13) in (5) as

$$\overline{P(w,k)} = \int_{-\infty}^{\infty} \int_{-\infty}^{\infty} p[u(x - Vt + a) - u(x - Vt - a)]\, \mathrm{e}^{-i(wt - kx)}\, \mathrm{d}x\, \mathrm{d}t \tag{15}$$

Then, (15) can be converted to a single integral with respect to t as follows:

$$\begin{aligned} \overline{P(w,k)} &= \int_{-\infty}^{\infty} \int_{Vt - a}^{Vt + a} p\mathrm{e}^{-i(wt - kx)}\, \mathrm{d}x\, \mathrm{d}t \\ &= 2p \int_{-\infty}^{\infty} \mathrm{e}^{-it(w - kV)} \frac{\sin(ka)}{k}\, \mathrm{d}t \end{aligned} \tag{16}$$

In simplifying the above expression, non-existence of the two unit step functions in the ranges $x < (Vt - a)$ and $x < (Vt + a)$ and Euler's relationship have been used.

Then by using the definition of the Fourier transform of any constant A given below:

$$\int_{-\infty}^{\infty} A e^{-iwt} dt = 2\pi A \delta(w) \tag{17}$$

(16) can be simplified to yield the following closed-form solution in terms of the Dirac delta function.

$$\overline{P(w,k)} = 4\pi p \frac{\sin(ka)}{k} \delta(w - kV) \tag{18}$$

The result obtained in (18) can be utilized in (13) to obtain the closed-form solution for the stress vector as

$$[\overline{P_1}] = 4\pi p \frac{\sin(ka)}{k} \begin{bmatrix} \mu\delta(w - kV) \\ 0 \\ i\delta(w - kV) \end{bmatrix} \tag{19}$$

Furthermore, by combining (14) and (19), the complete stress vector shown in (6) or (12) can now be written as

$$[\overline{P(\omega,k)}] = 4\pi p \frac{\sin(ka)}{k} [-\mu\delta(\omega - kV), 0, i\delta(\omega - kV), 0, 0, \ldots, 0, 0] \tag{20}$$

Inverse Fourier transform of the displacement vector

Due to the sparse nature of the force vector in (20), any jth surface displacement vector $[U_j]$ can be expressed in (12) only in terms of $[P_j]$ as

$$[\overline{U_j}] = [K_j^*]^{-1} [\overline{P_1}] \tag{21}$$

The matrix in (21) can be constructed simply by isolating the 3×3 partition formed by columns 1–3 and rows $(3j - 2)$–$(3j)$ of the inverse of the global stiffness matrix in (12). In most common pavement design procedures, although the stresses and deflections are obtained assuming the one-layer theory of elasticity, the authors assume three layers representing the asphalt wearing course, the base and the subgrade in the numerical illustrations presented in this paper.

In view of the numerical formulations encountered in Steps 4 and 5 of the layers stiffness procedure, it is convenient at this stage to denote $[K_j^*]^{-1}$ with its 3 column vectors as

$$[K_j^*]^{-1} = [\overline{C_{j1}(k,w)}, \overline{C_{j2}(k,w)}, \overline{C_{j3}(k,w)}] \tag{22}$$

since k and ω are the only variables in the layer stiffness expressions. Substitution of (19) and (22) into (21) produces

$$[\overline{U_j(w,k)}] = 4\pi p \delta(w - kV) \frac{\sin(ka)}{k} [-\mu \overline{C_{j1}(k,w)} + i \overline{C_{j3}(k,w)}] \tag{23}$$

Finally, (23) can be used in (7) to execute Step 5 of the layer stiffness procedure:

$$[U_j(t,x)] = \frac{p}{\pi} \int_{-\infty}^{\infty} \delta(w - kV) \frac{\sin(ka)}{k} [-\mu \overline{C_{j1}(k,w)} + i \overline{C_{j3}(k,w)}] e^{ik(\omega t - kx)} dk \tag{24}$$

Recalling that $\delta(\omega - kV)$ is non-zero only for $\omega = kV$, (24) can be reduced to

$$[U_j(t,x)] = \frac{p}{\pi}\int_{-\infty}^{\infty} \frac{\sin(ka)}{k}\,[-\mu\overline{C_{j1}(k)} + \mathrm{i}\,\overline{C_{j3}(k)}]\,\mathrm{e}^{\mathrm{i}k(Vt-x)}\,\mathrm{d}k \tag{25}$$

with single variable (k) functions $C_{j1}(k)$ and $C_{j3}(k)$ replacing the functions $C_{j1}(k, kv)$ and $C_{j3}(k, kv)$.

A close observation of (25) reveals that it is in fact an expression for the inverse Fourier transform (IFT) of $(2p\sin(ka)/k)[-\mu\overline{C_{j1}(k)} + \mathrm{i}\,\overline{C_{j3}(k)}]$. This fact can be further illustrated by performing a change of variables as

$$X = Vt - x \tag{26}$$

which simplifies (25) to

$$[U_j(X)] = 2p\,\frac{1}{2\pi}\int_{-\infty}^{\infty} \frac{\sin(ka)}{k}\,[-\mu\overline{C_{j1}(k)} + \mathrm{i}\,\overline{C_{j3}(k)}]\,\mathrm{e}^{\mathrm{i}kX}\,\mathrm{d}k \tag{27}$$

In fact, the new variable X is physically meaningful as it defines location of the point of interest w.r.t. the centre of the moving contact patch (Figure 2). Hence, X must solely govern the response of the pavement at any location in space (x) and any time (t) under steady conditions. Accordingly, (27) can be more concisely written in its final form as

$$[U_j(X)] = 2p\,\mathrm{IFT}\left[\left(\frac{\sin(ka)}{k}\right)(-\mu\overline{C_{j1}(k)} + \mathrm{i}\,\overline{C_{j3}(k)})\right] \tag{28}$$

PREDICTION OF DYNAMIC DEFLECTIONS AND STRESSES

Expression (28) derived above can now be used to predict the dynamic displacements at significant surfaces such as the pavement surface ($j = 1$) and the base/subgrade interface ($j = i + 1$). Moreover, as it is commonly practiced in structural analysis, the known deflections can be used to predict the stresses at any interface by substitution in the relevant local layer stiffness matrices such as those in (9)–(11).

NUMERICAL RESULTS

$[C_{j1}]$ and $[C_{j3}]$ column vectors in (28) will in general not be simple algebraic functions. Hence, a Fast Fourier Transformation (FFT) was found to be the most efficient means of executing (28). For this purpose, the discrete form of (27) can be written for a $2N$ number of k values spaced apart at intervals of k_0 as

$$[U_j(X)] = 2p\,\frac{k_0}{2\pi}\sum_{-N}^{(N-1)} \frac{\sin(nk_0a)}{nk_0}\,[-\mu\overline{C_{j1}(nk_0)} + \mathrm{i}\,\overline{C_{j3}(nk_0)}]\,\mathrm{e}^{\mathrm{i}nk_0X} \tag{29}$$

and the corresponding X domain for $2N$ discrete values will be defined by

$$X = \frac{\pi n}{Nk_0}$$

thus producing the limits of X as

$$-\frac{\pi}{k_0} \leqslant X < \frac{\pi}{k_0}$$

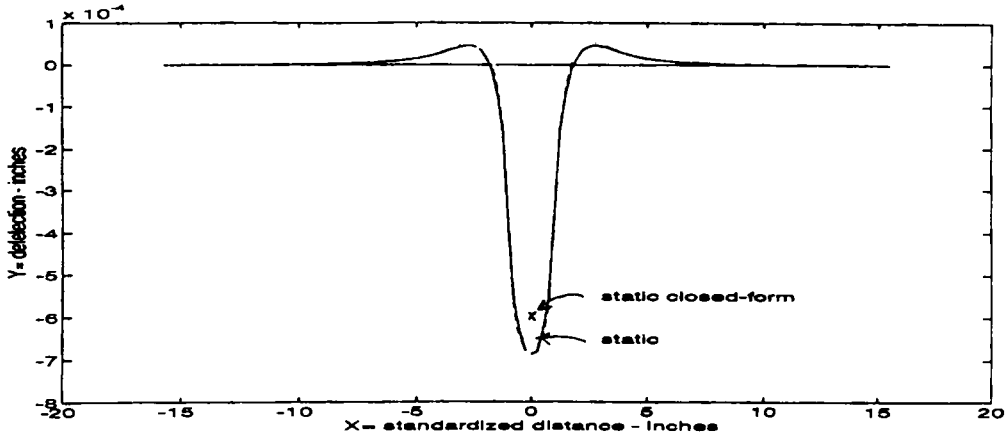

Figure 3. Comparison of homogeneous numerical and closed-form deflections

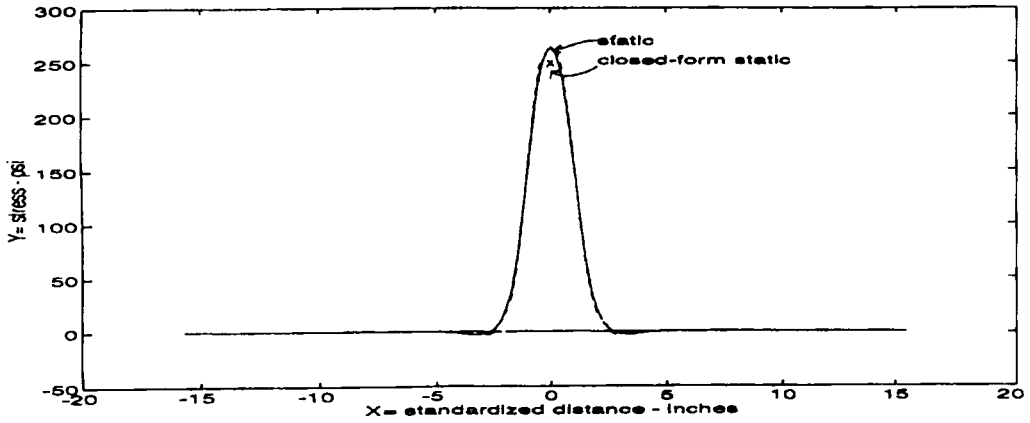

Figure 4. Comparison of homogeneous numerical and closed-form stresses

The above expressions indicate the FFT algorithm used in the numerical illustrations in this section.

Case 1: Comparison with closed-form solutions

In order to compare the numerical results with static elastic closed-form solutions, a 300 psi vertically distributed load placed on a 2 in thick homogeneous layer having an elastic modulus of 50 000 psi and a Poisson ratio of 0·4 overlying an incompressible layer was investigated. Figure 3 illustrated the agreement between the numerical results and the closed-form surface deflection. Furthermore, Figure 4 depicts the vertical static stress at a depth of 1 in, compared to the corresponding closed-form solution of 252 psi.[8]

In addition, the authors reviewed a case involving a two-layer system for comparison with closed-form solutions under static conditions. The static surface deflection due to a 300 psi vertical strip footing placed on a 9·0 in layer (elastic modulus 200 000 psi and Poisson ratio 0·4)

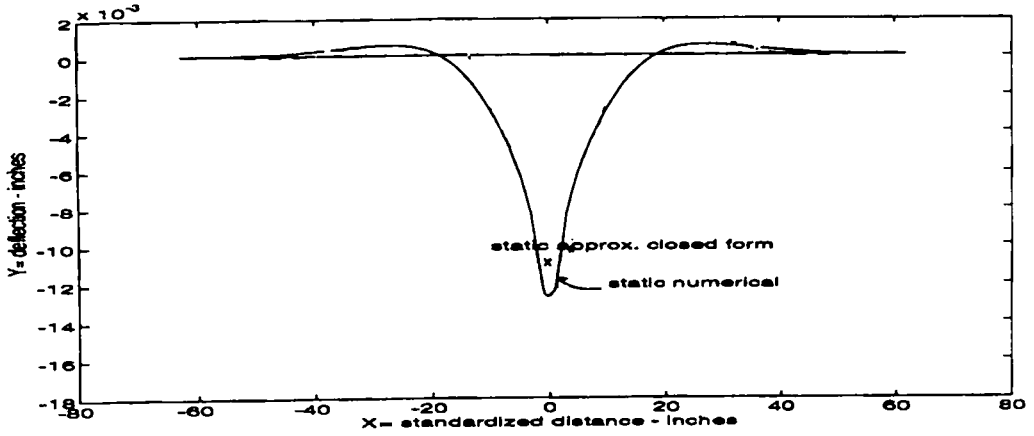

Figure 5. Comparison of two-layer numerical and closed-form deflections

Table I. Data used for sample load cases

	Load intensity	300 psi	
	Velocity*	3464 in/s (197 mph)	
	Footprint length ($2a$)	4 in	
	k_0 interval	0·05 (FFT in (29))	
	Range ($2N$)	64 (FFT in (29))	
	pavement	base	subgrade
Shear modulus	74 074 psi	11 111 psi	7 407 psi
Lame's constant	172 840 psi	25 926 psi	17 284 psi
Poisson's ratio	0·35	0·35	0·35
Layer thickness	4·0 m	8·0 in	8·0 in†
Weight density	0·1 psi	0·08 psi	0·07 psi

* This value was one-half of the average shear wave velocity of the base and subgrade
† In the numerical formulation, subgrade width was considered as the maximum of the depth where (11a) is satisfied or twice the base width.

overlying an infinitely thick softer layer (elastic modulus 50 000 psi and Poisson ratio 0·4) was evaluated to be approximately 0·01 in.[8] This is compared to the corresponding static solution obtained by the numerical solution, in Figure 5.

Case 2: Spatial and temporal variation of dynamic effects

In order to exhibit the model predictions, the surface and interface deflections as well as subgrade stresses were determined for different load cases from FFT output. The relevant strip loading, geometric and material data used are found in Table I. Figures 6 and 7 demonstrate the pavement surface and base/subgrade interface deflections due to a 300 psi vertically distributed load simulated to roll by the superposition of vertical and horizontal loads corresponding to a μ factor of 0·2. Furthermore, Figure 8 shows the vertical stresses induced by the rolling effect of the above load at the base/subgrade interface.

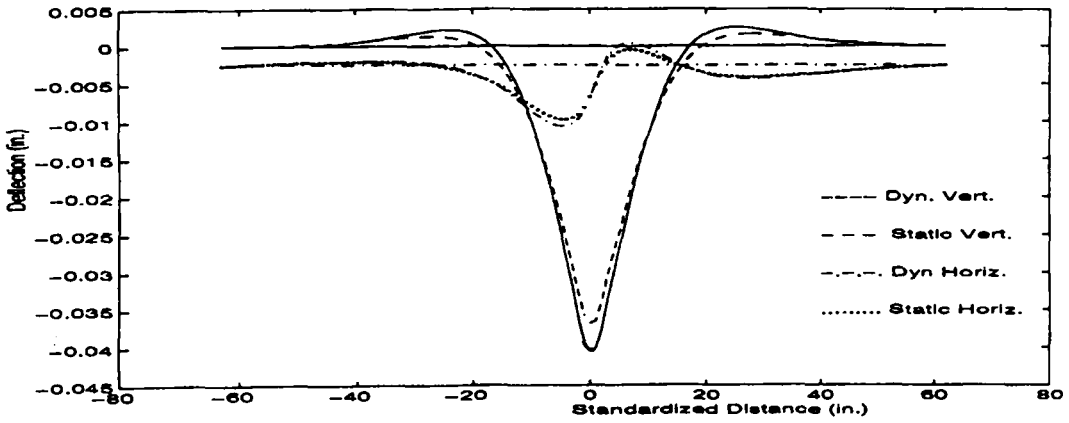

Figure 6. Pavement surface deflections due to a rolling line load

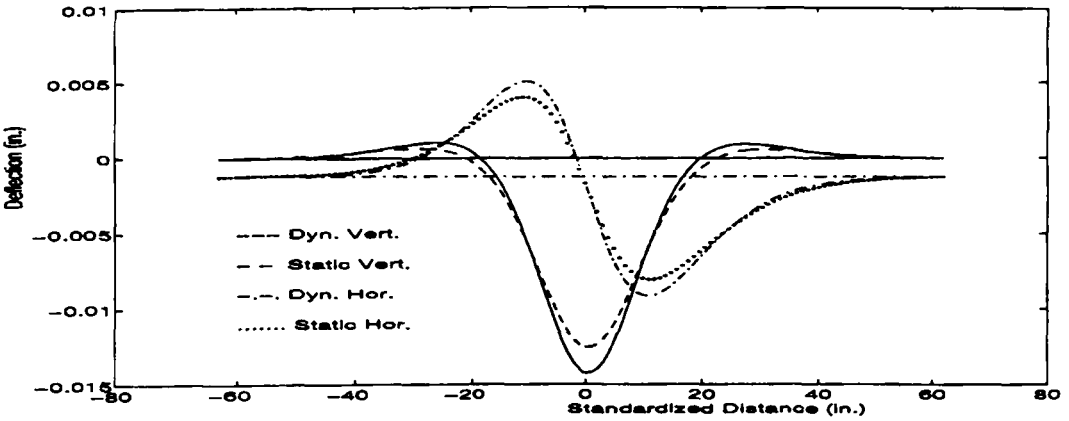

Figure 7. Base/subgrade interface deflections due to a rolling line load

Although the dependent variable is indicated as X, the same plots can be made to reveal the actual spatial distribution of the deflections at a given time or the time variation of the deflections at a particular point by manipulating (26). As an example, if $t = 0$, (26) yields $X = -x$, thereby exhibiting the variation of *initial* ($t = 0$) deflections around the load. On the otherhand, if x is set to zero, (26) produces $X = Vt$ making the same plots the variations of deflections at the *origin* with respect to a multiple of time. X is denoted as the 'standardized distance' in Figures 6–8 since it indicates the distance from the centre of the moving load to the point of interest, at any time t.

Case 3: Effects of variation of pavement thickness, velocity and subgrade stiffness

Extensive trials involving the variation of a number of variables revealed the existence of three convenient non-dimensional parameters. They are (1) ratio of the maximum dynamic deflection (or stress) to the maximum static deflection (or stress); (2) ratio of the footprint length ($2a$) to the asphalt thickness (a_1) (Figure 9); and (3) ratio of the base thickness (a_2) to the asphalt thickness

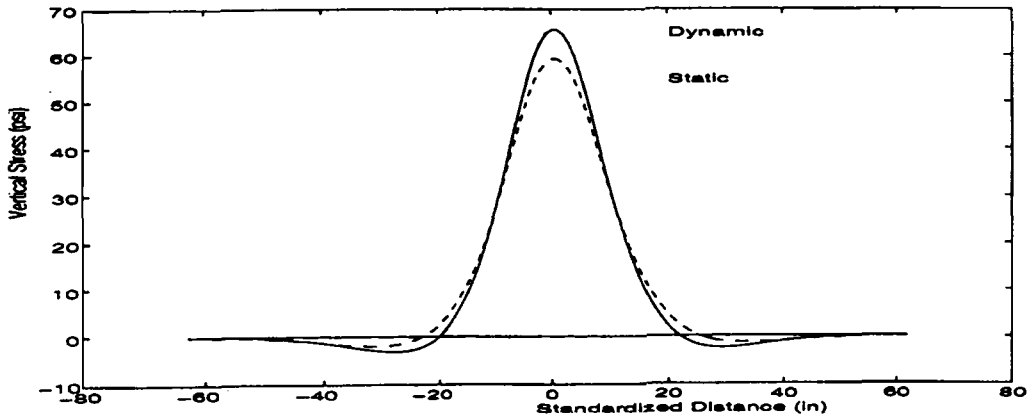

Figure 8. Vertical stresses at the base/subgrade interface due to rolling load

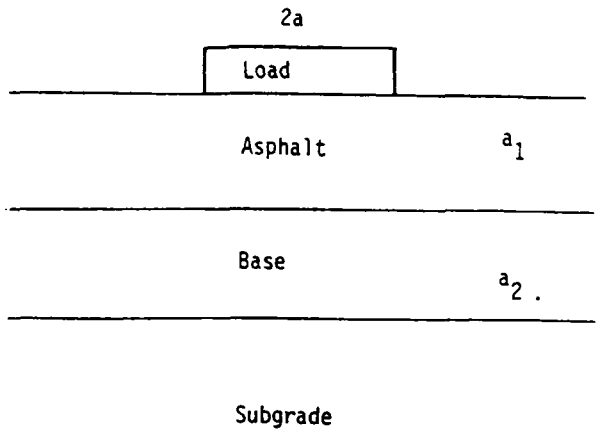

Figure 9. Typical asphalt pavement cross-section

(a_1) (Figure 9). Hereafter, they will be designated respectively, as 'the dynamic effect', 'the relative footprint length' and 'the relative base thickness', for convenience. Since, there are many established methods to obtain the *static* deflections and stresses on layered elastic systems, one will be able to scrutinize the dynamic deflections and stresses by solely employing the above 'dynamic effect'. Also, because the base material used for pavements is usually good-quality granular material, the base modulus was considered to be a constant at 30 000 psi to avoid complexity in the parametric study.

Figure 10 shows the variation of the dynamic effect of rolling with the rolling speed and relative footprint length for a modular ratio ($E_{\text{asphalt}}/E_{\text{subgrade}}$) of 1/10 and a relative base thickness of 2. Firstly, it is seen that the dynamic effect has only a minimal increase with increasing relative footprint length for a given rolling speed. On the other hand, the dynamic effect becomes pronounced only when the rolling speed approaches the average shear wave velocity of the base and the subgrade. Since the shear wave velocities of base and subgrade material were in the same range, their average was used as a comparison base for load velocity.

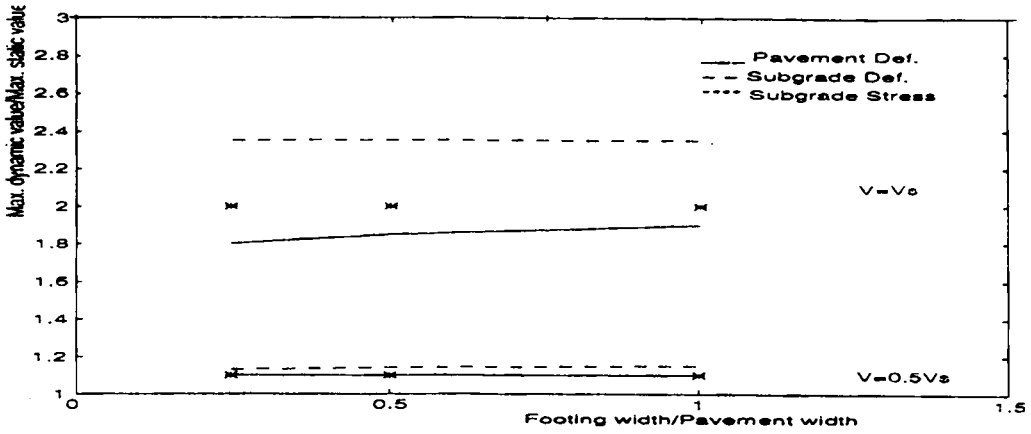

Figure 10. Variation of dynamic effect due to change of rolling speed (V) and relative footprint length ($2a/a_1$) (E_p = 200000 psi, E_s = 20000 psi, base thickness/asphalt thickness = 2)

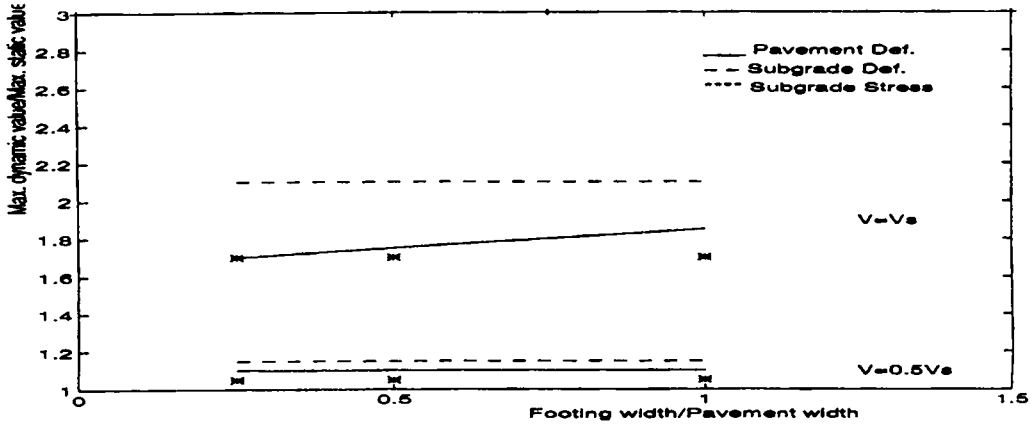

Figure 11. Variation of dynamic effect due to change of rolling velocity and relative footprint width ($2a/a_1$) (E_p = 200000 psi, E_s = 10000 psi, base thickness/asphalt thickness = 2)

Figure 11 is a similar plot where the subgrade modulus has been reduced while keeping the asphalt modulus constant (200000 psi), thereby reducing the modular ratio to 1/20. Figure 12, on the other hand, depicts the dynamic effects under the same moduli ratio (1/20) obtained by keeping the subgrade modulus constant (20000 psi) while increasing the asphalt modulus. Comparison of Figure 10–12 shows that the dynamic effects can be reduced by reducing the moduli ratio. However, Figures 11 and 12 show that increasing the asphalt modulus has a greater impact on the dynamic effects than decreasing the subgrade modulus.

The plot shown in Figure 13 was obtained when a similar study was done under a relative base thickness of 3 while maintaining the modular ratio at 1/10. As expected, comparison of Figure 10 and 13 shows that dynamic effects are more remarkable when the relative thickness of the asphalt layer is reduced when compared to the base and the subgrade.

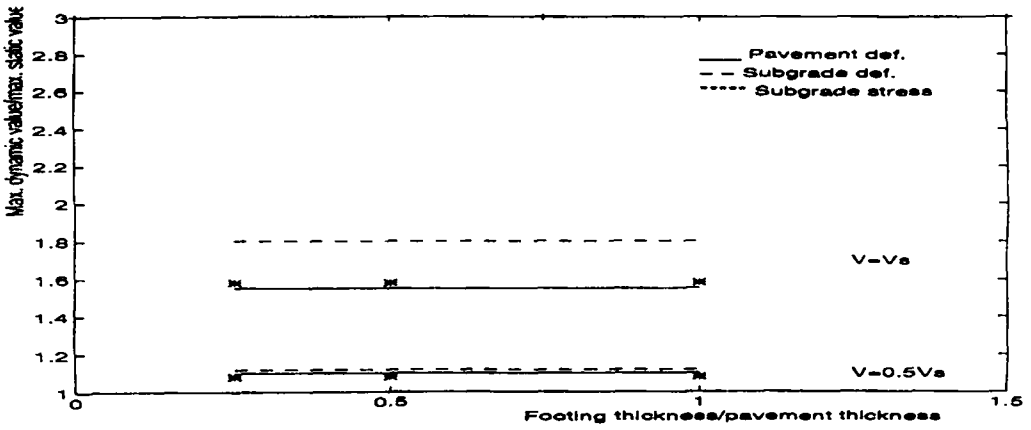

Figure 12. Variation of dynamic effect due to change of rolling velocity and relative footprint width ($2a/a_1$) (E_p = 400000 psi, E_s = 20000 psi, base thickness/asphalt thickness = 2)

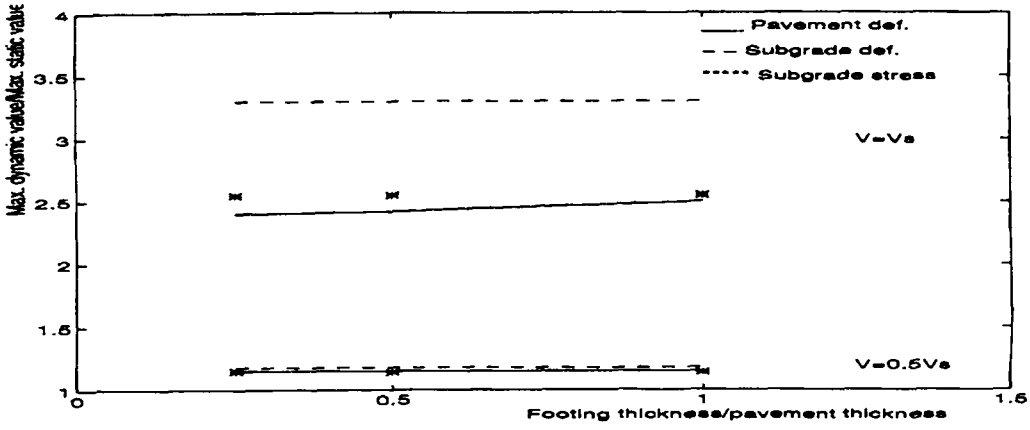

Figure 13. Variation of dynamic effect due to change of rolling velocity and relative footprint width (E_p = 200000 psi, E_s = 20000 psi, base thickness/asphalt thickness = 3)

DISCUSSION

Application to wheels rolling on pavements

One limitation of this model is that its predictions for infinite footings overestimate the stresses and deflections on the central vertical longitudinal plane of a finite wheel footprint. However, using a static distributed load on a homogeneous medium, it can be shown that this error can be eliminated by confining the predictions to depths within one-half of the wheel width as follows.

Figure 14 shows the variation of the static elastic vertical stress influence factor (I) defined by (30) at any depth (z) vertically under the centre of a rectangular footprint ($B \times L$) carrying a uniformly distributed load of p:

$$\sigma_v = pI \tag{30}$$

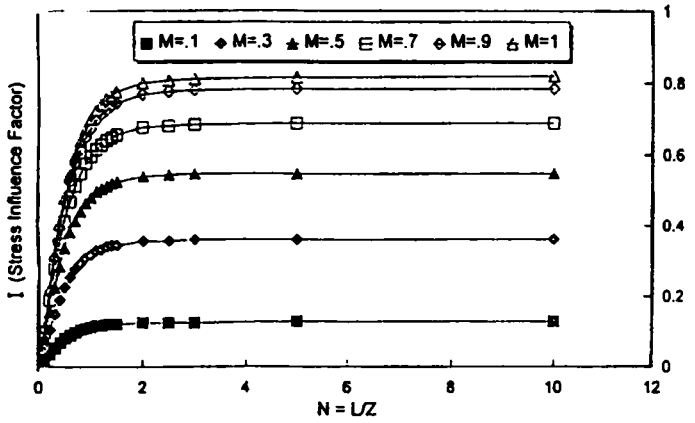

Figure 14. Variation of elastic vertical stress influence factor (I) at depth z under a rectangular footprint with non-dimensionalized size $M(=L/z) \times N(=B/z)$.

It is seen that for a given footprint length of L and a depth of z (i.e. at constant M) any significant vertical stress increase cannot be achieved by increasing the footprint width beyond $2z$ (*or* $N = B/z > 2$).

A similar situation can be expected for lateral stresses. Therefore, based on the generalized Hooke's law, one can deduce similar results for deflections as well.[8] Furthermore, the analytical results presented here shows that dynamic effects are not very pronounced until the rolling speed approaches the average base/subgrade shear wave velocity (Figures 10–13). Hence, one can conclude that overprediction of stresses and deflections by this infinite strip footing model can be eliminated by choosing a wide wheel such as an aircraft tire, and limiting the depth of prediction to regions close to the pavement (which certainly includes the pavement surface!).

Effects of viscoelastic behaviour of asphalt concrete

An application of this model is cited from pavement analysis since it is commonplace to apply layered elastic theory to asphalt pavements and soils, especially when back-computing the layer moduli in the use of non-destructive testing for pavement evaluation. The authors emphasize that predicted results are applicable to any pavement exhibiting linear elastic behaviour. Although linear elastic properties are used in most pavement designs, asphalt properties can generally be more realistically characterized by viscoelastic models, in view of their time-dependent behaviour. However, if the viscoelastic relaxation time for asphaltic concrete is relatively small, the viscous response may not be significant. In cases where the viscous response is expected to be signficant, the layer stiffness procedure can be modified to incorporate damping properties by means of complex shear moduli and Lame's constants as follows:

$$E^* = E(1 + \lambda\omega i] \tag{31}$$

where E^* the complex modulus, E is the elastic modulus (used in the spring element of Kelvin's model), λ the damping coefficient (used in the dashpot element of Kelvin's model) and ω the angular frequency of load application.

Accordingly, the shear modulus and Lame's constant can be modified to include damping by their complex counterparts as

$$G^* = \frac{E^*}{2(1+\mu)}$$

and

$$L^* = \frac{\mu E^*}{(1-2\mu)(1+\mu)}$$

On the other hand, in scrutinizing the time-dependent effects, one can speculate that while the time history of deflection at a given pavement location is certainly prolonged by viscoelastic behaviour, the maximum deflection will significantly reduce, especially when the load moves at a high velocity. This has been illustrated by comparing the elastic and viscoelastic strains induced on the surface of a homogeneous infinite layer by a steadily moving distributed load, by utilizing a single Kelvin element to represent the considered location on the pavement (see the appendix).

Execution of inverse Fourier transformation

In executing the numerical solution, the authors discovered that the cutoff wave number ($2N$) in (29) depends on the loading and layer geometry. Hence, the determination of the appropriate sampling rate (k_0) and cutoff wave number, which are designated in Table I as the interval and the maximum range in the wave-number domain, can most efficiently be performed based on a trial basis. By sequentially increasing the cutoff wave number and decreasing the sampling rate, the numerical results for static loads were made to converge on the closed-form solutions (Figures 3–5). It was also found that consideration of sampling intervals of less than 0·05 cycles/in and wavelengths of less than 1/64 in was insignificant to the convergence of dynamic resutls as well.

CONCLUSION

A numerical procedure has been formulated to predict the magnitude of stresses and deflections due to a moving vertical or horizontal strip load at any desired depth of a layered elastic system using a layer stiffness method. Using this technique, the rolling action of a wide wheel on an asphaltic pavement can be approximately simulated by the superposition of vertical and horizontal load cases.

A major limitation in this simulation is that the contact between even wide pneumatic wheel loads and asphaltic pavements is limited only to a finite patch. However, it was shown that the *static* vertical stresses (and hence the deflections) caused by a strip footing on any vertical plane parallel to the direction motion are mainly due to a finite portion of the load immediately surrounding the given plane. Furthermore, the model predictions (Figures 10–13) indicate that until the rolling velocity reaches the shear wave velocity range of the base and the subgrade, the dynamic stress and deflection distributions are only slight modifications of their static counterparts. Based on the above arguments, one can conclude that the numerical solutions furnished in this paper provides a valuable insight into the distribution of stresses and deflections due to the actual motion of a wide wheel contact patch on a layered system such as an asphaltic pavement. Possible deviations anticipated due to viscous dampling in asphalt are also discussed with the aid of a simple viscous damping model involving a Kelvin element.

The execution ease and the practicality of the proecdure were vividly displayed by the numerical illustrations. The expected symmetry of vertical deflections and the skew-symmetry of

horizontal deflections are observed from the numerical results. Moreover, comparison of the subgrade and pavement deflections indicate that a substantial portion of the vertical surface deflection originates in the relatively compressible subgrade. Similarly, the horizontal deflections in the subgrade and pavement are roughly equal in magnitude. This is due to the fact that the attenuation of horizontal stress at the subgrade depths is offset by its relatively low compressibility.

The numerical results for the static load cases are in excellent agreement with the corresponding closed-form solutions for both stresses and deflections. A notable observation is the increase of the magnitude of deflections and stresses of the elastic foundation when the distributed load travels with a steady velocity. This is in contrast to the predictions of Davies and Mamlouk[9] for *harmonic loads* applied on pavements, where the dynamic response was shown to be slightly lower in magnitude than the static response. Inclusion of damping could have played a major role in this reduction.

A parametric study revealed three non-dimensional quantities that will be useful in predicting the dynamic effects for a pavement system with given stiffness properties. They are (1) the relative length of the footprint compared to asphalt thickness; (2) the relative thickness of the base compared to the asphalt thickness; and (3) the ratio of rolling speed to average shear wave velocity of the base and subgrade. A significant finding was that the dynamic effects can be reduced by increasing asphalt stiffness and thickness with respect those of the base and the subgrade.

The authors also found that the results were practically unaltered by using the simplified stiffness matrices with algebraic expressions given in Reference 1. This proves the effectiveness of Lysmer and Waas[7] linearization even for the crude layering considered in the numerical illustrations presented here.

ACKNOWLEDGEMENT

The authors wish to thank The University of South Florida graduate student Sujeeva Weerasuriya and Saman Thilakasiri for their help in some of the computational work.

APPENDIX

If one assumed the vertical footing stress distribution in Figure 2 which is mathematically defined by (8c) to be applied on a Kelvin element (a spring E in parallel with a dashpot Λ) representing a homogeneous semi-infinite asphalt pavement layer, the following stress-strain equation can be written:

$$\lambda \frac{d\varepsilon}{dt} + E\varepsilon = p[u(x - Vt + a) - u(x - Vt - a)] \tag{32}$$

(A1) can be solved by employing an integration factor of

$$e^{\int (E/\lambda) dt}$$

Thus, one obtains

$$\varepsilon e^{(E/\lambda t)} = \frac{p}{\lambda} \int_{-\infty}^{t} e^{(E/\lambda t)} [u(x - Vt + a) - u(x - Vt - a)] \, dt \tag{33}$$

For a given position x, the difference in step functions in the integrand has a value of 1·0 in the range

$$\left(\frac{x-a}{V}\right) < t < \left(\frac{x+a}{V}\right)$$

and 0 everywhere else. Hence, the strain can be expressed as

$$\varepsilon e^{(E/\lambda t)} = \frac{p}{\lambda} \int_{(x-a)/V}^{t} e^{(E/\lambda t)} dt \tag{34}$$

for

$$\left(\frac{x-a}{V}\right) < t < \left(\frac{x+a}{V}\right) \tag{35}$$

and

$$\varepsilon e^{(E/\lambda t)} = \frac{p}{\lambda} \int_{(x-a)/V}^{(x-a)/V} e^{(E/\lambda t)} dt \tag{36}$$

for

$$t > \left(\frac{x+a}{V}\right) \tag{37}$$

Thus, the simplified strain is expressed as

$$\varepsilon = \frac{p}{E}\left[1 - \exp\left(\frac{E}{\lambda}\left(\frac{x-a}{V} - t\right)\right)\right] \tag{38}$$

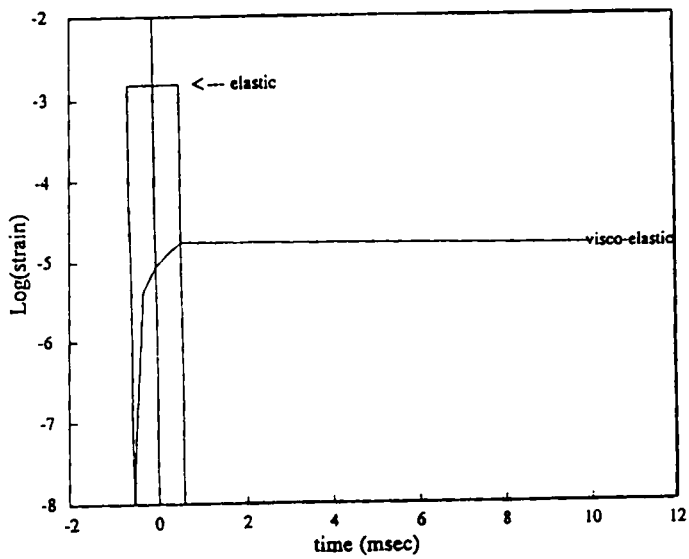

Figure 15. Comparison of elastic and viscoelastic strains in a semi-infinite medium due to a moving strip load.

for the time range in (34), and

$$\varepsilon = \frac{p}{E} \exp\left[\left(\frac{E}{\lambda}\left(\frac{x-a}{V} - t\right)\right) - \exp\left(\frac{E}{\lambda}\left(\frac{x-a}{V} - t\right)\right)\right] \tag{39}$$

for the time range in (36).

Finally, the time variation of the viscoelastic strain at $x = 0$ due to a moving strip load is plotted in Figure 15 using the data in Table 1. As for the damping constant of the asphalt medium, a typical value of 20000 psi was used, thus producing a retardation time (T) of 0.1 s. Figure (15) also shows the corresponding strains obtained without the dashpot element, thus clearly illustrating that for considerably high velocities, the maximum strain in a homogeneous viscoelastic medium does not reach anywhere near the maximum elastic strain. However, the relatively insignificant strains induced in the viscoelastic medium can persist for a very long time as seen in Figure 15.

REFERENCES

1. E. Kausel and J. M. Roesset, 'Stiffness matrices for layered soil', *Bull. Seismol. Soc. Amer.*, **71**, (1981).
2. E. Kausel and R. Peek, 'Dynamic loads in the interior of a layered stratum', *Bull. Seismol. Soc. Amer.* **72**, (1982).
3. E. Kausel, Discussion to 'Dynamic strip analysis of surface foundations', Earthquake engineering and Structural Dynamics, Vol. 16, 1988 by Chow, Y. K., Swaddiwudhipong, S., and Lim, S. A., Vol. 18, pp. 1081–1083, 1989.
4. M. Mamlouk and T. Davies, 'Elasto-dynamic analysis of pavement deflections', *J. Transport. Eng. ASCE*, **110**, (1984).
5. P. E. Sebaaly, T. Davies and M. S. Mamlouk, 'Dynamics of falling weight deflectometer', *J. Transport. Eng. ASCE*, **111**, (1985).
6. P. E. Sebaaly and M. S. Mamlouk, 'Development of dynamic fatigue failure criterion', *J. Transport. Eng. ASCE*, **114**, (1988).
7. J. Lysmer and G. Waas, 'Shear waves in plane infinite structures', *J. Eng. Mech Div. ASCE*, **98**, 85–105 (1972).
8. H. F. Winterkorn and H. Fang, *Foundation Engineering Handbook*, Van Nostrand Reinhold Company, New York, 1975.
9. T. G. Davies and M. S. Mamlouck, 'Theoretical response of multilayer pavement systems to dynamic nondestructive tersting', *Transportation research Record* 1002, 1985.
10. Y. H., Huang, *Pavement Analysis and Design*, Prentice-Hall, Englewood Cliffs, NJ, 1993.